Nanoscale

Cite this: *Nanoscale*, 2012, **4**, 183

www.rsc.org/nanoscale

PAPER

A magnetically separable photocatalyst based on nest-like γ-Fe_2O_3/ZnO double-shelled hollow structures with enhanced photocatalytic activity†

Yu Liu,[a] Le Yu,[b] Yong Hu,*[a] Changfa Guo,[a] Fumin Zhang[a] and Xiong Wen (David) Lou*[b]

Received 16th August 2011, Accepted 8th October 2011
DOI: 10.1039/c1nr11114k

Magnetic nest-like γ-Fe_2O_3/ZnO double-shelled hollow nanostructures have been successfully synthesized *via* a multi-step process. The materials have been thoroughly characterized by different techniques. These interesting nest-like hollow nanostructures are composed of ZnO nanoflakes grown on the surface of γ-Fe_2O_3 hollow spheres. Importantly, these magnetic hollow nanostructures show very high visible-light photocatalytic activity for the degradation of different organic dyes including methylene blue (MB), Rhodamine-B (RhB), and methyl orange (MO). It is further demonstrated that these γ-Fe_2O_3/ZnO hybrid photocatalysts are highly stable and can be used repeatedly.

1. Introduction

During the past few decades, many research efforts have been concentrated on the environmental use of semiconductor photocatalysts for the degradation of toxic organic compounds which are discharged from industries and households.[1] TiO_2 based materials are widely used as important photocatalysts due to their high photosensitivity and nontoxic nature.[2,3] Recently, it has been reported that ZnO can also be used as a major component of photocatalysts due to its similar bandgap energy (3.2 eV). More importantly, ZnO has several advantages including lower cost, high quantum efficiency and high photocatalytic activity.[4] However, the photocatalytic activity of ZnO should be further enhanced for large scale use. Therefore, various methods have been developed to reduce the recombination rate of photogenerated electrons and holes in ZnO based photocatalysts. Hybrid semiconductor nanostructures have been proven very efficient for the removal of organic pollutants from water. The combination of two semiconductors with different energy levels may form an ideal system to cause a rapid photoinduced charge separation and decreased chance of recombination of electron–hole pairs by the synergetic effect.[5,6] The enhanced photocatalytic efficiency is explained by a fast transfer of photogenerated electrons and holes from one semiconductor to another. For example, one-dimensional (1D) ZnO/ZnS core–shell nanostructures manifest significantly higher photocatalytic activity than pure ZnO tested under the same conditions.[7]

It is well known that separation of photocatalysts from large volumes of reaction solutions requires a largish expense. Therefore, it is highly desirable to develop photocatalysts that can be easily collected for re-use. Magnetic nanoparticles, which can be collected easily by applying an external magnetic field, offer some unbeatable ease for separation and recycling of photocatalysts. Thus, incorporating a magnetic component into the photocatalytically active materials is an attractive route to fabricate magnetically separable photocatalysts. The magnetic component might not only prevent the agglomeration of the catalyst nanoparticles during recovery,[8] but also offer some synergetic enhancement of the catalytic activity by forming the hybrid structure. Along this line, several magnetically separable core–shell structured photocatalysts have been designed, including Fe_3O_4/TiO_2, Fe_3O_4/ZnO or Fe_3O_4/CdS nanocomposites, which possess enhanced photocatalytic activity.[9–11]

As a unique class of nanostructured materials, inorganic hollow structures have attracted enormous research efforts owing to their technological importance in a wide range of applications.[12,13] Various kinds of single- or multi-phase hollow nanostructures, such as ZnO, Fe_2O_3, and Fe_3O_4/TiO_2 hollow spheres,[14–16] have been obtained by different approaches. Among them, Fe_2O_3 hollow spheres, with high light-harvesting efficiency, have recently been used as a photocatalyst with high photocatalytic activity.[17,18] Herein we design a multi-step method to fabricate novel γ-Fe_2O_3/ZnO nest-like double-shelled hollow nanostructures. The procedure of this method is described in

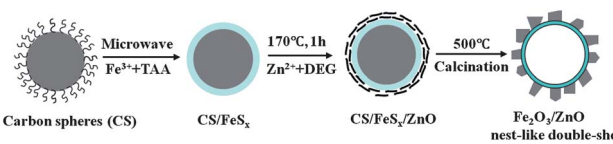

Scheme 1 Schematic illustration of the formation of γ-Fe_2O_3/ZnO nest-like double-shelled hollow nanostructures.

[a]*Institute of Physical Chemistry, Zhejiang Normal University, Jinhua, 321004, P.R. China. E-mail: yonghu@zjnu.edu.cn*
[b]*School of Chemical and Biomedical Engineering, Nanyang Technological University, 70 Nanyang Drive, Singapore, 639798, Singapore. E-mail: xwlou@ntu.edu.sg*

† Electronic supplementary information (ESI) available: XRD/TEM/schematic illustration of charge transfer. See DOI: 10.1039/c1nr11114k

Scheme 1. In the first step, a layer of FeS_x is coated on the surface of colloidal carbon spheres by a microwave irradiation technique.[17] Then, the as-prepared C/FeS_x nanocomposites and zinc acetate dehydrate are mixed in diethylene glycol (DEG). The mixture is then refluxed at 170 °C for 1 h to obtain the sandwiched nanostructures of C/FeS_X/ZnO. Finally, the composite is calcined in air to obtain γ-Fe_2O_3/ZnO nest-like double-shelled hollow nanostructures. These novel structured magnetic composites show greatly enhanced visible-light photocatalytic activity and excellent recyclability for the degradation of different organic dyes including methylene blue (MB), rhodamine B (RhB), and methyl orange (MO).

2. Experimental section

2.1. Synthesis of C/FeS_x core–shell hybrid spheres

The C/FeS_x core–shell hybrid spheres were prepared following a previous method.[17] Briefly, 3.96 g of glucose was dissolved into 40 mL of distilled water to form a clear solution that was then transferred into a 50 mL Teflon-lined stainless steel autoclave. After hydrothermal treatment at 180 °C for 8 h, carbon spheres are obtained. In the next step, 0.01 mol of $Fe(NO_3)_3 \cdot 9H_2O$ was added into a round-bottom flask and dissolved in a solvent containing 10 mL of ethanol and 10 mL of distilled water, forming a clear solution. 25 mg of the as-prepared carbon spheres was added into the above solution and was well dispersed with the assistance of sonication for 10 min. The mixture was maintained at 60 °C for 12 h to achieve adsorption/desorption equilibrium. The solid material was then collected by centrifugation. To remove possible superfluous cations and anions, the obtained product was washed with ethanol and distilled water for three times, and then dried at 80 °C for 4 h. The above-obtained sample and 0.01 mol of thioacetamide (TAA) were placed in a microwave refluxing system irradiated at 400 W for 30 min, which resulted in formation of carbon/FeS_x core–shell composite spheres. After collection by centrifugation, the as-prepared products were washed with ethanol and distilled water for three times before drying at 80 °C for 4 h.

2.2. Synthesis of nest-like double-shelled γ-Fe_2O_3/ZnO hollow nanostructures

0.025 g of the as-prepared C/FeS_x precursor was added into a round-bottom flask and dispersed in 20 mL of DEG with the assistance of sonication for 10 min. Then, 0.05 g of zinc acetate dihydrate was added into the above mixture under vigorous stirring for 30 min, and the temperature of reaction solution was increased to 170 °C and aged for 1 h.[19] After collection by centrifugation, the as-prepared sandwich-structured C/FeS_x/ZnO spheres were washed with distilled water and absolute ethyl alcohol for three times before being dried at 80 °C for 4 h. The final γ-Fe_2O_3/ZnO nest-like double-shelled hollow nanostructures were obtained by calcining the C/FeS_x/ZnO composite at 500 °C in static air for 2 h.

2.3. Characterization

Powder X-ray diffraction (XRD) measurements of the samples were performed with a Philips PW3040/60 X-ray diffractometer using Cu Kα radiation at a scanning rate of 0.06 deg s^{-1}. Scanning electron microscopy (SEM) analysis was performed with a Hitachi S-4800 scanning electron micro-analyzer with an accelerating voltage of 15 kV. Transmission electron microscopy (TEM) and high-resolution transmission electron microscopy (HRTEM) analyses were conducted using a JEM-2100F field emission TEM. Samples for TEM measurements were prepared by dispersing the products in ethanol and placing several drops of the suspension on a holey carbon net supported on copper grids. Further evidence for the composition of the product was inferred from X-ray photoelectron spectroscopy (XPS), using an ESCALab MKII X-ray photoelectron spectrometer with Mg Ka X-ray as the excitation source. The photoluminescence (PL) spectra were recorded on an Edinburgh FLSP920 fluorescence spectrometer with an excitation wavelength of 325 nm and the absorption spectra were measured using a PerkinElmer Lambda 900 UV-vis spectrophotometer at room temperature.

2.4. Photocatalytic activity measurement

Photocatalytic activities of γ-Fe_2O_3/ZnO nest-like double-shells were evaluated by the degradation of different organic dyes including MB, RhB, and MO under visible light irradiation using a 500 W Xe lamp with a cutoff filter at 420 nm. The reaction cell was placed in a sealed black box with an opening on the top, and the cutoff filter was placed to provide visible-light irradiation. In a typical process, 0.05 g of photocatalyst was added into 100 mL of solution containing one of the above organic dyes with a concentration of 5 mg L^{-1}. After being dispersed in an ultrasonic bath for 5 min, the solution was stirred for 2 h in the dark to reach the adsorption/desorption equilibrium between the catalyst and the dye. Then, the suspension was exposed to the visible light irradiation.[20] The samples were collected at given time intervals. After the separation of photocatalyst by an external magnetic field, the dye concentration was measured by using UV-vis spectroscopy. To study the regeneration and reusability of the photocatalyst, the photocatalyst was collected by a permanent magnet and then washed with ethanol and distilled water for three times before being redispersed in a fresh dye aqueous solution for use in the next cycle.

3. Results and discussion

X-Ray powder diffraction analysis was carried out to investigate the crystal phases of the as-synthesized products. A typical XRD pattern of the final products is shown in Fig. 1. The diffraction peaks marked by asterisks correspond to cubic γ-Fe_2O_3 (JCPDS card no. 39-1346) and those marked by triangles can be indexed to the hexagonal ZnO (JCPDS card no. 36-1451). Because the (440) peak of γ-Fe_2O_3 is very close to the (103) diffraction peak of ZnO, two peaks are overlapped together and cannot be easily distinguished. No peaks due to other undersigned phases are observed.

Fig. 2a shows a typical SEM image of uniform C/FeS_x obtained by microwave irradiation at 400 W and the average diameter is found to be about 1 μm. The morphology of the as-prepared C/FeS_x/ZnO spheres obtained by a refluxing process is shown in Fig. 2b. From the high-magnification image (Fig. 2b, inset), one can distinctly observe the growth of sheet-like

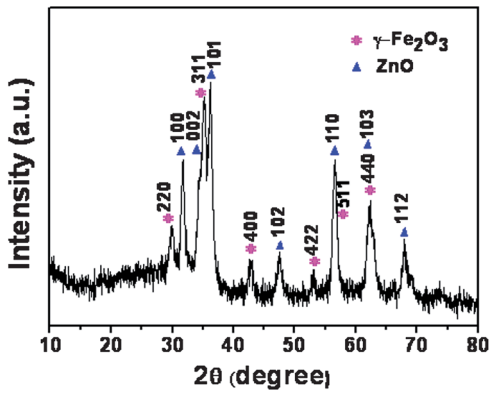

Fig. 1 XRD pattern of γ-Fe_2O_3/ZnO nest-like hollow nanostructures.

structures on the surface of the spheres. The formation of outer ZnO nanoplatelets may be ascribed to the following reactions:

$$Zn(CH_3COO)_2 + xH_2O \xrightarrow{\Delta} Zn(OH^-)_x(CH_3COO^-)_{2-x} + xCH_3COOH \quad (1)$$

$$Zn(OH^-)_x(CH_3COO^-)_{2-x} \xrightarrow{\Delta} ZnO + (x-1)H_2O + (2-x)CH_3COOH \quad (2)$$

Eqn (1) is the hydrolysis reaction of $Zn(OAc)_2$ to form metal complexes, which will further dehydrate to form pure ZnO (eqn (2)) during the aging process.[21] The morphology of the γ-Fe_2O_3/ZnO nest-like double-shelled hollow nanostructures obtained after calcination is shown in Fig. 2c, which reveals many irregular ZnO flakes grown on the surface of γ-Fe_2O_3 hollow spheres. Fig. 2d shows a broken structure, and the TEM image (Fig. 2e) further reveals that the as-prepared products are hollow structures. The process of calcination in air allows the oxidation of FeS_x to form γ-Fe_2O_3,[17] at the same time leads to the formation of bigger ZnO nanoflakes.[22] The heterojunction region between γ-Fe_2O_3 and ZnO is shown in the HRTEM image (Fig. 2f). The XRD pattern and TEM image of the as-prepared magnetic photocatalyst after the photocatalytic test are shown in Fig. S1 and S2 (ESI†). Remarkably, there is no significant change in both composition and structure. This indicates that the γ-Fe_2O_3/ZnO nest-like hollow nanostructures have high chemical and structural stability.

It is difficult to clearly distinguish the γ-Fe_2O_3 and Fe_3O_4 phases from the XRD pattern. Thus, the chemical composition of the products is further analyzed by XPS. The typical survey spectrum of the γ-Fe_2O_3/ZnO nest-like hollow nanostructures is depicted in Fig. 3a, which shows the presence of O, C, Zn, and Fe elements. The high-resolution spectrum of Fe is given in Fig. 3b, the electron binding energy of Fe (2p3/2, 710.5 eV and 2p1/2, 724.3 eV) is in good agreement with the literature and is consistent with that of γ-Fe_2O_3.[23] Besides, the shake-up satellite structures are also observed at the higher binding energy sides of the main peaks, indicated by arrows. These satellite peaks are the fingerprints of the electronic structures of Fe^{3+} and indicate that Fe^{2+} is absent.[23,24] Fig. 3c displays a high-resolution spectrum of Zn, the peaks at 1021.8 eV and 1045.0 eV correspond to Zn 2p3/2 and 2p1/2, respectively. It should be noted that the binding energy of Zn shows a positive shift compared with that of pure ZnO (1022.0 eV).[25] The difference may be ascribed to the electron transfer from the Fermi level of ZnO to the Fermi level of γ-Fe_2O_3.[7] The O 1s peak (Fig. 3d) can be deconvoluted into three

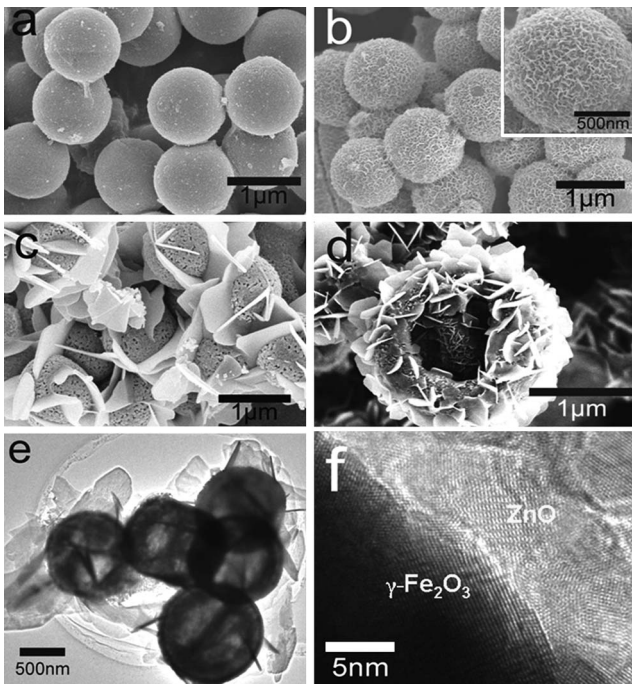

Fig. 2 Typical SEM images of the as-prepared C/FeS_x core–shell spheres (a) C/FeS_x/ZnO spheres (b) and a higher magnification image (inset). (c and d) SEM images of γ-Fe_2O_3/ZnO nest-like hollow nanostructures. (e) TEM and (f) HRTEM images of γ-Fe_2O_3/ZnO nest-like hollow nanostructures.

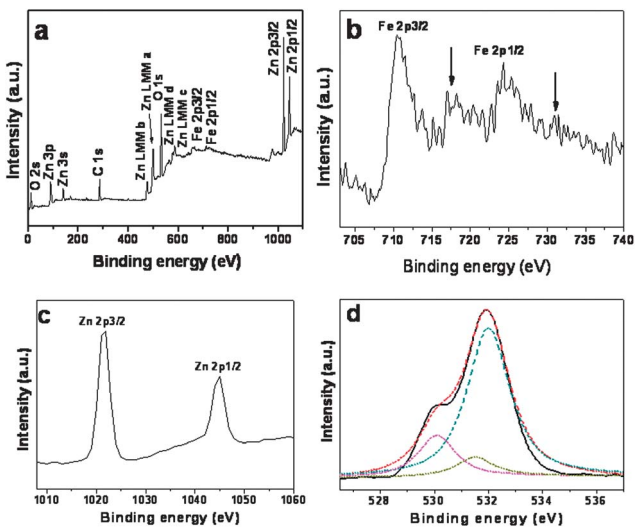

Fig. 3 XPS spectra of as-prepared γ-Fe_2O_3/ZnO nest-like hollow nanostructures: (a) survey spectrum, (b) Fe (2p) binding energy spectrum, (c) Zn (2p) binding energy spectrum, and (d) O (1s) binding energy spectrum.

peaks by the XPS peak fitting program. The peaks at 530.3 and 531.9 eV can be attributed to O in γ-Fe_2O_3 and ZnO respectively,[26,27] and the peak at 531.5 eV should be assigned to surface oxygen, which can be described as surface oxygen species "O^-".[28]

To investigate the optical properties of the as-prepared magnetic γ-Fe_2O_3/ZnO nest-like hollow structures, the PL spectrum is recorded at room temperature. For comparison, the PL spectrum of commercial ZnO powder is also obtained at the same conditions. Both PL spectra are shown in Fig. 4. The UV emission located at 382 nm is the band-edge emission resulting from the recombination of free excitons, and the broad green emission centered at 496 nm is caused by the radiative recombination of the photogenerated holes with electrons around the surface oxygen vacancy. In comparison with the PL spectrum of commercial ZnO, the UV emission of γ-Fe_2O_3/ZnO nest-like hollow nanostructures is enhanced, while the defect emission is suppressed. This phenomenon can be attributed to the passivation of γ-Fe_2O_3 nanoparticles, and a similar observation has been reported previously.[23]

The photocatalytic activities of the as-prepared magnetic γ-Fe_2O_3/ZnO nest-like hollow structures are evaluated by the degradation of organic dyes including MB, RhB and MO under visible-light irradiation. Fig. 5a shows the relative concentration (C/C_0) of MB as a function of time, where C is the concentration of MB at the irradiation time t and C_0 is the concentration of the dye before irradiation. Three measurements are carried out by using different photocatalysts, commercial ZnO and γ-Fe_2O_3/ZnO nest-like hollow structures, as well as the control experiment without any photocatalyst. After visible-light irradiation for 50 min, 95.2% of MB is degraded in the presence of γ-Fe_2O_3/ZnO hollow nanostructures, while approximately 87.6% of MB is decomposed using commercial ZnO as the photocatalyst. This indicates that this γ-Fe_2O_3/ZnO photocatalyst is only slightly more active than commercial ZnO nanoparticles. However, the superior photocatalytic activity of this γ-Fe_2O_3/ZnO photocatalyst becomes apparent for degradation of other dyes. Fig. 5b shows the photodegradation behavior of RhB catalyzed by blank, commercial ZnO nanoparticles, and γ-Fe_2O_3/ZnO nest-like hollow nanostructures under visible light illumination. About 91.1% of RhB is photodegraded using γ-Fe_2O_3/ZnO hybrids after 50 min of irradiation, compared to only 51.5%

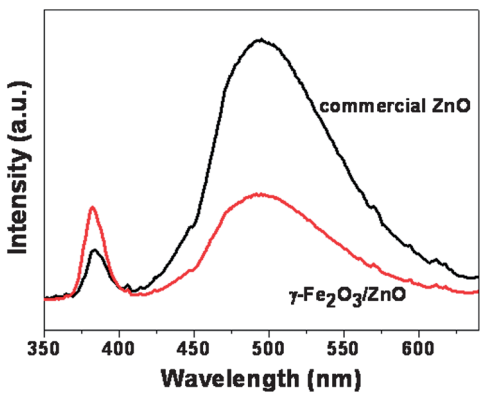

Fig. 4 PL spectra of the γ-Fe_2O_3/ZnO nest-like hollow nanostructures and commercial ZnO powder.

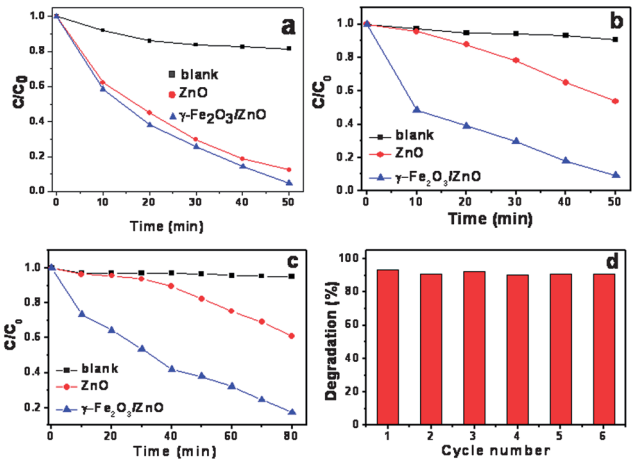

Fig. 5 Photodegradation of (a) MB, (b) RhB and (c) MO under visible-light irradiation by blank, commercial ZnO nanoparticles, and γ-Fe_2O_3/ZnO nest-like hollow nanostructures. (d) 6 cycles of degradation of MB using γ-Fe_2O_3/ZnO nest-like hollow nanostructures as the photocatalyst.

when using commercial ZnO nanoparticles. Fig. 5c presents the photodegradation behavior of MO irradiated by visible-light. As can be seen, almost 82.5% of MO can be removed within 80 min, compared to only 39.5% with commercial ZnO nanoparticles during the same time period. These results show that γ-Fe_2O_3/ZnO nest-like hollow structures possess enhanced visible-light photocatalytic activity for degradation of the above dyes. The schematic diagram representing the charge transfer process in γ-Fe_2O_3/ZnO hybrid structures is illustrated in Scheme S1 (see ESI†). The superior photocatalytic activity of these hybrid structures is mainly due to the suitable heterojunctions formed between the two semiconductors with different energy levels. Specifically, Fe(III) in Fe_2O_3 can be easily reduced to Fe(II), and it is deduced that in the presence of Fe_2O_3 the electrons in the conduction band of ZnO can be easily accepted by Fe_2O_3. Additionally, it is very important for the suppression of the recombination of photogenerated electron–hole pairs. In this hybrid structure, the accumulated electrons in the conduction band of Fe_2O_3 can be transferred to the molecular oxygen adsorbed on the surface of mixed semiconductor systems.[29–31] The surface area of the as-prepared γ-Fe_2O_3/ZnO nest-like hollow structures and the commercial ZnO powder is measured by the BET method using an ASAP2020 sorptometer. The γ-Fe_2O_3/ZnO nest-like hollow structures have a specific surface area of 42.1 $m^2\ g^{-1}$, and it is only 3.0 $m^2\ g^{-1}$ for the commercial ZnO powder. In addition, the particle size of commercial ZnO powder is about 41.8 nm estimated using the Debye–Scherrer equation. Thus, the enhanced photocatalytic activity might be related to the unique nest-like hollow structure of the γ-Fe_2O_3/ZnO, which gives a large surface area.

We have also evaluated the reusability of the magnetically separable γ-Fe_2O_3/ZnO photocatalyst. For this, the photocatalyst is repeatedly used for the photodegradation of MB. As shown in Fig. 5d, after six runs of photodegradation of MB, the photocatalytic activity of the γ-Fe_2O_3/ZnO hybrid structures does not show obvious deterioration. It clearly demonstrates that these magnetic photocatalysts are quite stable and have great application potential in water treatment.

4. Conclusions

In summary, we have designed a magnetically separable photocatalyst based on novel γ-Fe_2O_3/ZnO nest-like hollow nanostructures by a multi-step process. First, C/FeS_x core–shell spheres were obtained *via* a rapid microwave-assisted reaction. Then, a layer of ZnO was further deposited on the surface of C/FeS_x spheres by a simple sol–gel method forming C/FeS_x/ZnO spheres. After calcination of the C/FeS_x/ZnO composite at 500 °C in static air, the nest-like γ-Fe_2O_3/ZnO hollow nanostructures were obtained. The as-prepared γ-Fe_2O_3/ZnO nest-like hollow nanocomposites exhibit excellent recyclable photocatalytic activity for the degradation of different organic dyes including MB, RhB and MO under visible-light irradiation. These novel magnetically separable photocatalysts may find important applications in the treatment of polluted wastewater and environmental cleaning.

Acknowledgements

Financial support from Natural Science Foundation of China (21171146; 20806075), Zhejiang Provincial Natural Science Foundation of China (Y4110304) and Zhejiang Qianjiang Talent Project (2010R10025) is gratefully acknowledged. X.W. Lou greatly acknowledges the financial support from Energy Research Institute @ NTU (ERIAN).

Notes and references

1 C. Galindo, P. Jacques and A. Kalt, *J. Photochem. Photobiol., A*, 2001, **141**, 47.
2 J. G. Yu, L. J. Zhang, B. Cheng and Y. R. Su, *J. Phys. Chem. C*, 2007, **111**, 10582.
3 K. Maeda and K. Domen, *Chem. Mater.*, 2010, **22**, 612.
4 S. Sakthivel, B. Neppolian, M. V. Shankar, B. Arabindoo, M. Palanichamy and V. Murugesan, *Sol. Energy Mater. Sol. Cells*, 2003, **77**, 65.
5 L. Y. Ying, S. Y. Dong, J. H. Sun, J. L. Feng, Q. H. Wu and S. P. Sun, *J. Hazard. Mater.*, 2010, **179**, 438.
6 Z. Y. Zhang, C. L. Shao, X. H. Li, L. Zhang, H. M. Xue, C. H. Wang and Y. C. Liu, *J. Phys. Chem. C*, 2010, **114**, 7920.
7 Y. Hu, H. H. Qian, Y. Liu, G. H. Du, F. M. Zhang, L. B. Wang and X. Hu, *CrystEngComm*, 2011, **13**, 3438.
8 L. Wang, H. W. Wei, Y. G. Fan, X. Gu and J. H. Zhan, *J. Phys. Chem. C*, 2009, **113**, 14119.
9 J. S. Chen, C. P. Chen, J. Liu, R. Xu, S. Z. Qiao and X. W. Lou, *Chem. Commun.*, 2011, **47**, 2631.
10 R. Y. Hong, S. Z. Zhang, G. Q. Di, H. Z. Li, Y. Zheng, J. Ding and D. G. Wei, *Mater. Res. Bull.*, 2008, **43**, 2457.
11 X. W. Liu, Z. Fang, X. J. Zhang, W. Zhang, X. W. Wei and B. Y. Geng, *Cryst. Growth Des.*, 2009, **9**, 197.
12 X. W. Lou, L. A. Archer and Z. C. Yang, *Adv. Mater.*, 2008, **20**, 3987.
13 F. Caruso, R. A. Caruso and H. Mohwald, *Science*, 1998, **282**, 1111.
14 H. S. Qian, G. F. Lin, Y. X. Zhang, P. Gunawan and R. Xu, *Nanotechnology*, 2007, **18**, 355602.
15 S. W. Cao and Y. J. Zhu, *J. Phys. Chem. C*, 2008, **112**, 6253.
16 S. H. Xuan, W. Q. Jiang, X. L. Gong, Y. Hu and Z. Y. Chen, *J. Phys. Chem. C*, 2009, **113**, 553.
17 Y. Liu, Y. Hu, C. F. Guo and X. Hu, *J. Am. Ceram. Soc.*, 2011, **94**, 1667.
18 Y. Hu, H. S. Qian, T. Mei, J. Guo and T. White, *Mater. Lett.*, 2010, **64**, 1095.
19 H. M. Cheng, H. C. Hsu, S. L. Chen, W. T. Wu, C. C. Kao, L. J. Lin and W. F. Hsieh, *J. Cryst. Growth*, 2005, **277**, 192.
20 Y. Hu, Y. Liu, H. Qian, Z. Li and J. Chen, *Langmuir*, 2010, **26**, 18570.
21 Y. Hu, H. S. Qian, C. F. Guo and T. Mei, *CrystEngComm*, 2010, **12**, 2687.
22 Y. Hu, T. Mei, J. Guo and T. White, *Inorg. Chem.*, 2007, **46**, 11031.
23 P. Wu, N. Du, H. Zhang, L. Jin and D. Yang, *Mater. Chem. Phys.*, 2010, **124**, 908.
24 Y. J. Chen, F. Zhang, G. G. Zhao, X. Y. Fang, H. B. Jin, P. Gao, C. L. Zhu, M. S. Cao and G. Xiao, *J. Phys. Chem. C*, 2010, **114**, 9239.
25 J. Zhang, X. H. Liu, L. W. Wang, T. L. Yang, X. Z. Guo, S. H. Wu, S. R. Wang and S. M. Zhang, *Nanotechnology*, 2011, **22**, 185501.
26 X. P. Dong, H. R. Chen, W. R. Zhao, X. Li and J. L. Shi, *Chem. Mater.*, 2007, **19**, 3484.
27 N. M. Bahadur, T. Furusawa, M. Sato, F. Kurayama and N. Suzuki, *Mater. Res. Bull.*, 2010, **45**, 1383.
28 G. Wu, X. Y. Tana, G. Y. Li and C. W. Hu, *J. Alloys Compd.*, 2010, **504**, 371.
29 W. Yan, H. Q. Fan and C. Yang, *Mater. Lett.*, 2011, **65**, 1595.
30 S. Sakthivel, S. U. Geissen, D. W. Bahnemann, V. Murugesan and A. Vogelpohl, *J. Photochem. Photobiol., A*, 2002, **148**, 283.
31 J. G. Yu, X. X. Yu, B. B. Huang, X. Y. Zhang and Y. Dai, *Cryst. Growth Des.*, 2009, **9**, 1474.